"Self-biased nonreciprocal microstrip phase shifter on magnetic nanowired substrate suitable for gyrator applications"

Hamoir, Gaël ; De La Torre Medina, Joaquin ; Piraux, Luc ; Huynen, Isabelle

ABSTRACT

Magnetic nanowired substrates (MNWS) have been used for the fabrication of a planar nonreciprocal microstrip device. It shows a differential phase shift of 300 degrees${cdot}$ cm^{-1} at Ka -band without requiring the application of a dc bias magnetic field, and making it suitable for miniaturized gyrator applications. The nonreciprocal operation is achieved by loading the device with nanowires of different ferromagnetic materials. This allows to control the phase velocity of the microwave signal passing through the device by virtue of the spatial variation of the MNWS permeability. The measured microwave performances of the device have been reproduced with excellent accuracy using a proposed analytical model based on an effective medium theory and useful for the prediction of further tunable capabilities.

CITE THIS VERSION

Hamoir, Gaël ; De La Torre Medina, Joaquin ; Piraux, Luc ; Huynen, Isabelle. *Self-biased nonreciprocal microstrip phase shifter on magnetic nanowired substrate suitable for gyrator applications.* In: *IEEE Transactions on Microwave Theory and Techniques*, Vol. 60, no. 7, p. 2152-2157 (July 2012) http://hdl.handle.net/2078.1/112128 -- DOI : 10.1109/TMTT.2012.2195016

Self-Biased Nonreciprocal Microstrip Phase Shifter on Magnetic Nanowired Substrate Suitable for Gyrator Applications

Gaël Hamoir, Joaquin De La Torre Medina, Luc Piraux, and Isabelle Huynen, *Senior Member, IEEE*

***Abstract*—Magnetic nanowired substrates (MNWS) have been used for the fabrication of a planar nonreciprocal microstrip device. It shows a differential phase shift of 300 degrees·cm^{-1} at Ka-band without requiring the application of a dc bias magnetic field, and making it suitable for miniaturized gyrator applications. The nonreciprocal operation is achieved by loading the device with nanowires of different ferromagnetic materials. This allows to control the phase velocity of the microwave signal passing through the device by virtue of the spatial variation of the MNWS permeability. The measured microwave performances of the device have been reproduced with excellent accuracy using a proposed analytical model based on an effective medium theory and useful for the prediction of further tunable capabilities.**

***Index Terms*—Alumina, ferromagnetic nanowires, gyrator, integrated, microstrip, nonreciprocal, phase shifter, self-biased.**

I. Introduction

CURRENT passive nonreciprocal microwave devices based on ferrite materials [1]–[3] have received great attention in the last decades and are nowadays employed in a wide spectrum of applications. However, classical devices present limitations since their frequency of operation is usually limited to the X-band due to the low saturation magnetization value of ferrites, and they must be biased by an external magnetic field, which represents a limitation of size reduction. Self-biased hexaferrites may be used for nonreciprocal millimeter-wave devices [2], [4]. They usually require hybrid topology, for example,the hexaferrite disc is mechanically inserted in a circular cavity drilled in a low-loss insulating substrate supporting RF access lines, requiring bonding wires to make the contact between hexaferrite cavity and planar accesses. As an alternative to overcome such limitations, novel nanocomposite materials based on arrays of magnetic nanowires (NWs) grown into nanoporous membranes have been proposed [5]–[9]: nanowired areas in the alumina substrate can easily be delimited by masking techniques during electrodeposition, enabling the coexistence in the same planar substrate of self-biased ferromagnetic and dielectric (insulating) zones, fully compatible with microstrip or coplanar waveguide technology. The high length-to-diameter aspect ratio of low-diameter NWs makes them self-biased magnetically along their axis due to shape anisotropy, and their frequency of operation lies above the X-band, up to 30 GHz in CoFe alloyed NW arrays. Nonreciprocal microwave devices based on MNWS have been the subject of recent works and include circulators [10]–[13], isolators [14], [15], and differential phase shifters [16], [17]. In microstrip-line topologies lying on a ferromagnetic or ferrite material, the microwave electric and magnetic field patterns are nonuniform by virtue of the edge-guided mode, since they are preferably concentrated near one long edge of the microstrip due to the coupling between the microwave signal traversing the microstrip and the gyromagnetic properties of the magnetized magnetic material [18]. This principle combined with an asymmetrical loading of the microstrip results in a nonreciprocal behavior, which has recently been applied to obtain differential phase-shift performances in MNWS [16], [17].

In this paper, we propose a nonreciprocal microstrip line (NRML) based on MNWS that have a large differential phase shift observed in absence of dc magnetic field and induced by a ferromagnetic resonance (FMR) transverse field displacement principle. The proposed device consists of a microstrip-line geometry on a single planar substrate filled with NWs of different magnetic alloys, namely, NiFe and CoFe. The nonreciprocal behavior of the present device is achieved by controlling the phase velocity of the microwave signal guided on the microstrip line via a variation of the MNWS permeability. As a result, a nonreciprocal differential phase shift up to 300 degrees·cm^{-1} is obtained at zero applied dc magnetic field, making the present device suitable for gyrator applications [19] and electronically scanned arrays antennas [20]. The simulated absorption and differential phase shift are in excellent agreement with the experimental results, and the proposed model allows to predict further tunable capabilities of the NRML presented in this work.

II. Device Topology and Fabrication

The MNWS is fabricated by three-probe electrodeposition of NiFe and CoFe NWs into 100-μm-thick commercial porous

Manuscript received August 29, 2011; revised March 21, 2012; accepted March 25, 2012. Date of publication June 04, 2012; date of current version June 26, 2012. This work was supported in part by the Interuniversity Attraction Poles Program (P6/42)-Belgian State-Belgian Science Policy. The work of J. De La Torre was supported by PROMEP and CONACYT under Grant PROMEP/103.5/11/2159 and Grant 166089, respectively, as well as UCL.

G. Hamoir and L. Piraux are with the Institute of Condensed Matter and Nanosciences (ICMN), Université Catholique de Louvain, B-1348, Louvain-la-Neuve, Belgium.

J. De La Torre Medina is with the Facultad de Ciencias Físico-Matemáticas, Universidad Michoacana de San Nicolás de Hidalgo, 58030 Morelia, Mexico.

I. Huynen is with the Institute of Information and Communications Technologies, Electronics and Applied Mathematics (ICTEAM), Université Catholique de Louvain, B-1348 Louvain-la-Neuve, Belgium.

Color versions of one or more of the figures in this paper are available online at http://ieeexplore.ieee.org.

Digital Object Identifier 10.1109/TMTT.2012.2195016

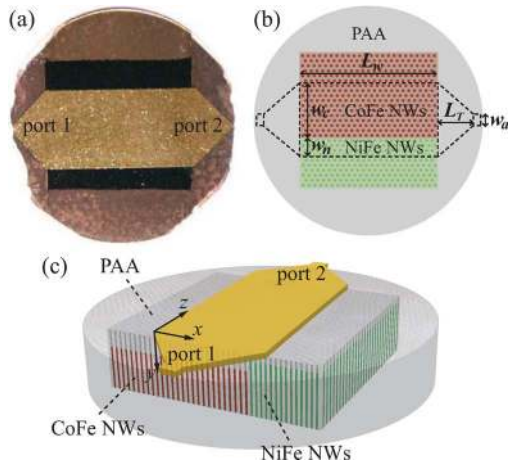

Fig. 1. (a) Photograph of the top view of the fabricated NRML. (b) Schematic 2-D view of the NRML showing the spatial arrangement of the areas with NWs and the microstrip line (dotted line) which is divided in two zones with widths $w_c = 4$ mm and $w_n = 0.5$ mm and length $L_w = 8$ mm over the zones with CoFe and NiFe grown at heights 0.68 and 0.84 of the membrane thickness, respectively. The width of the microstrip line is $w = w_c + w_n = 4.5$ mm and tapers to a width $w_a = 0.2$ mm at their two ports and its total length is $L = L_w + 2L_T = 12$ mm where $L_T = 2$ mm is the taper length. (c) Corresponding 3-D schematic view.

anodic alumina (PAA) membranes from Synkera [12] with pores diameter $d = 35$ nm and membrane porosity or NWs packing factor $P = 12\%$. A Cr(20 nm)/Au(600 nm) layer is evaporated onto one side of the membranes to serve as a cathode for electrodeposition and as a ground plane for the microwave measurements. NiFe and CoFe NWs are grown from the Cr/Au layer at the bottom of the porous membrane using the following electrolytes: 131.42 g l^{-1} $NiSO_4$ + 5.56 g l^{-1} $FeSO_4$ + 24.73 g l^{-1} H_3BO_3 with the pH adjusted to 3; and 80 g l^{-1} $CoSO_4$ + 40 g l^{-1} $FeSO_4$ + 30 g l^{-1} H_3BO_3 with the pH adjusted to 4, respectively. Electrodeposition of the NWs is done in potentiostatic mode at room temperature by applying potentials of -1 V for NiFe and -0.9 V for CoFe NWs.

The filling of the membranes with NWs is carried out in two steps with the purpose of obtaining two adjacent rectangular zones where CoFe and NiFe NWs are grown. In step one, electrodeposition of CoFe NWs takes place in a limited area with width greater than 4 mm and length $L_w = 8$ mm and NiFe NWs are subsequently electrodeposited in an area with width greater than 0.5 mm and length $L = 8$ mm just besides the one for the CoFe NWs. For the growth of NWs, a rubber mask with a rectangular hole through which the electrolytic solution is in contact with the porous membrane is placed into the electrolytic cell in order to accurately define the area where NiFe NWs are deposited into the membrane and to prevent their growth over the previously deposited CoFe NWs. The NWs height is determined from the time necessary to completely fill the porous membrane. Finally, a 4.5-mm-wide and 12-mm-long microstrip line is evaporated onto the side of the membrane opposite to the one with the previously evaporated cathode as seen in the NRML photograph of Fig. 1(a). The microstrip line is such that its long dimension is placed parallel to the junction of both zones of NWs and covers a width $w_c = 4$ mm of the CoFe area and $w_n = 0.5$ mm of the NiFe area as seen schematically in Fig. 1(b). Therefore, the microstrip line is 4.5 mm wide over the zones with NWs and tapers to a width $w_a = 0.2$ mm at their two ports, as shown schematically in the corresponding 2-D [see Fig. 1(b)] and 3-D [see Fig. 1(c)] views of the NRML shown in Fig. 1(a). The taper sections are added in order to facilitate the contact with the connectors of the test fixture used for the measurement and improve the matching of the wide NRML section to the 50-Ω reference impedance of the measuring equipment. A large width of the NRML is needed over the nanowired area to induce the field-displacement mechanism that will be detailed in Section III. The total length of the microstrip device is $L = L_w + 2L_T = 12$ mm with the addition of the taper length $L_T = 2$ mm.

III. Theoretical Predictions

A. Field-Displacement Mechanism

The nonreciprocal operation of the device of Fig. 1 is based on a transverse field displacement along the microstrip line, which is caused by the ferromagnetic materials beneath the microstrip. Contrary to previously reported NRML, where the nonreciprocal behavior depends on an asymmetrical filling with NWs of the same material [16], [17], the present device is nonreciprocal even if the MNWS is symmetrically filled with NWs. The principle of operation of the former depends on the strong variation of height profile of the NW array, which can be stairway-like [16] or gradient-like [17], and then on the resulting asymmetry of the substrate permittivity across the microstrip line. In the latter, the principle of operation arises from the asymmetry on the permeability tensor $\bar{\mu}_i$ in each zone, with $i = c$ for CoFe NWs or $i = n$ for NiFe NWs. In other words, in the present device, the permeability of the NWs is varied in order to control the phase velocity of the microwave signal passing through the microstrip line. As a consequence of the presence of ferromagnetic material, the y-component of the electric field E_{y_i} and the x-component of the magnetic field $H_{x_i} = (k_z/\omega\mu_o)E_{y_i}$ with $i = c, n$, are nonuniform across the x position of the transverse section of the microstrip line, which can be rewritten from Hines formalism [18] as

$$E_{y_c} = Ae^{-\alpha_c x}, \qquad \text{for} \quad 0 \le x \le w_c \tag{1}$$

$$E_{y_n} = Ae^{-\alpha_c w_c} e^{-\alpha_n (x - w_c)}, \qquad \text{for } w_c \le x \le w_n \tag{2}$$

In (1) and (2), $\alpha_i = j\kappa_i k_z/\mu_i$, where k_z is the propagation constant and $j\kappa_i$ and μ_i are the off-diagonal and diagonal components of the permeability tensors, respectively, for zones with CoFe ($i = c$) and NiFe ($i = n$) NWs and are given by [10]

$$\mu_i = 1 + 2\pi M_{s_i}\gamma P h_i f_i \left(f_i^2 - f^2\right)^{-1} \left(m_i^2 + 1\right) \tag{3}$$

$$\kappa_i = 4\pi M_{s_i}\gamma P h_i f \left(f_i^2 - f^2\right)^{-1} m_i. \tag{4}$$

In the previous equations $f_i = \gamma[H_{\mathrm{DC}} + 2\pi M_{s_i}(1 - 3P)] + j\alpha_{l_i} f$ is the FMR frequency, $m_i = M_i/M_{s_i}$ is the normalized magnetization along the y axis of the NWs, $\alpha_{l_i} = 1/(2\pi f \tau_i)$ is the damping factor, H_{DC} is the static field applied parallel to the y-axis of the NWs which in our case is set to zero, f is the

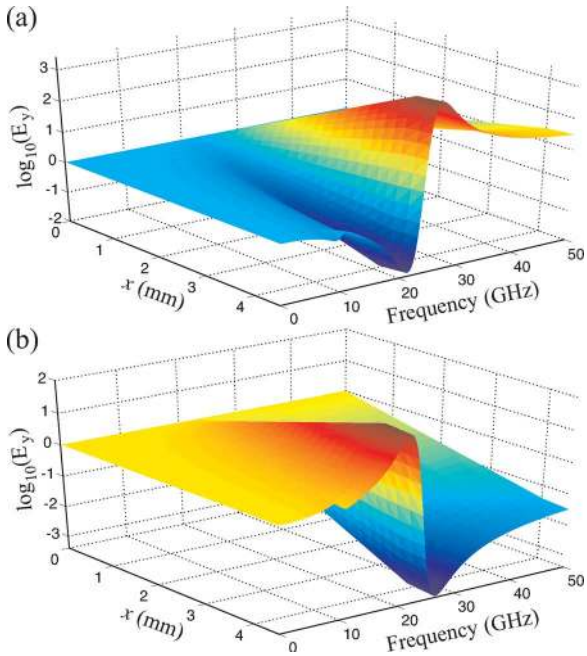

Fig. 2. 3-D view of the calculated electric field pattern E_y as a function of the x-position and the excitation frequency f at zero external bias field for (a) positive and (b) negative direction of propagation (or magnetization). Log magnitude of field is plotted for sake of clarity, after normalization for each frequency to its value at side edge of CoFe NW area ($x = 0$). As magnetic field H_x is proportional to E_y by the factor $k_z/\omega\mu_0$, its pattern looks identical to the E-field pattern after normalization.

microwave operation frequency, M_{s_i} is the saturation magnetization, $\gamma = 3$ GHz·kOe^{-1} is the gyromagnetic ratio, while P is the volumetric fraction of nanowires in the porous template. It is worth mentioning that the difference between the permeability tensors for the CoFe and NiFe NW zones arises from the differences between f_c and f_n and, more precisely, from M_{s_i} and τ_i, which have values $M_{s_c} = 1850$ emu·cm^{-3}, $M_{s_n} = 825$ emu·cm^{-3}, $\tau_c = 6.3 \times 10^{-11}$, and $\tau_n = 1.4598 \times 10^{-10}$. Equations (1)–(2) enable us to predict that the decay of field along the positive x-direction is different in the two zones because of the different permeabilities of the material, but also that this decay is reversed, i.e., occurring along the negative x-direction or, equivalently, causing amplification in the positive x-direction, when the direction of either propagation (fixing the sign of k_z, hence of α_i) or magnetization (fixing the sign of m_i) are inverted. The FMR mechanism implies that the sign of component κ_i is different below and above FMR frequency, meaning that the decay of the field is reversed from below-resonance to above-resonance frequency ranges. These predictions are illustrated and confirmed at Fig. 2, showing the field patterns simulated for the device presented in this paper, using (1)–(2).

The nonreciprocal behavior is achieved by combining this field-displacement mechanism with the change of permeability across the transverse section induced by the change of ferromagnetic material: as the field concentration in each zone depends on the propagation (or magnetization) direction, so will the effective permeability experienced by the microwave signal guided also depend on the microstrip line. Hence, its quasi-TEM propagation constant and characteristic impedance will depend on the sense of propagation (or magnetization), making the device nonreciprocal.

B. Quasi-TEM Nonreciprocal Transmission-Line Formalism

Using the effective medium approach, an analytical homogeneization formula is proposed for the effective permeability experienced by the signal for each direction of propagation (or magnetization), along positive $(+)$ or negative $(-)z$ (or y) axis:

$$\frac{1}{\mu_{\text{eff}}^{\pm}} = \frac{\int_0^{w_c} \frac{\mu_c}{\mu_c^2-\kappa_c^2} H_{x_c}^{\pm}(x)dx + \int_{w_c}^{w_n} \frac{\mu_n}{\mu_n^2-\kappa_n^2} H_{x_n}^{\pm}(x)dx}{\int_0^{w_c} H_{x_c}^{\pm}(x)dx + \int_{w_c}^{w_n} H_{x_n}^{\pm}(x)dx} \tag{5}$$

where the expression $(\mu_i^2 - \kappa_i^2)/\mu_i$ is effective permeabilities associated with quasi-TEM propagation in each ferromagnetic zone [21]. The use of inverted quantities is required in (5) because inductive contributions under the microstrip have to be considered in parallel and not in series [22]. Superscripts $\pm$ in the field variables indicate that (1)–(2) are used either with positive/negative values of propagation coefficient ($\Im(k_z) = \pm|\Im(k_z)|$) for positive value of m_i or with positive/negative values of $m_i (m_i = \pm|m_i|)$ for positive values of $\Im(k_z)$. From expression (5), nonreciprocal quasi-TEM complex propagation constants depending on direction of propagation (or magnetization), and associated characteristic impedances can be calculated as

$$k_{\pm} = j\frac{\omega}{c_o}\sqrt{\mu_{\text{eff}}^{\pm}\varepsilon_{\text{eff}}} \tag{6}$$

$$Z_{c\pm} = 377\frac{h}{w}\sqrt{\frac{\mu_{\text{eff}}^{\pm}}{\varepsilon_{\text{eff}}}} \tag{7}$$

where ε_{eff} is the equivalent effective permittivity of the nanowired substrate, function of the filling factor [23], w is the width of the microstrip over the nanowired area, and h is the thickness of the alumina substrate.

IV. Experimental Validation

The transmission coefficient $T_{\pm} = e^{-k_{\pm}L}$ in the forward $(+)$ and backward $(-)$ propagation directions has been simulated using the formalism summarized in the previous section at zero applied dc bias magnetic field ($H_{\text{DC}} = 0$). The S-matrix of the NRML section lying on the nanowired part of the substrate was calculated from $T_{\pm}$ and $Z_{c\pm}$ using the formalism proposed in [26] for nonreciprocal transmission lines. It was then transposed to the S-matrix referenced to the 50 Ω of the measuring equipment using classical S- to chain-matrix conversion formulas, and making a cascaded product of chain matrices of input taper, NRML nanowired section, and output taper, respectively. Microwave measurements are carried out in two-port configuration using a vector network analyzer (VNA) (Anritsu 37297C). The $(\pm)$ propagation directions in experiments correspond to propagation from port 1 to port 2 and from port 2 to port 1, respectively, as shown in Fig. 1(c). Fig. 3(a) shows, in both directions of propagation, the magnitude $S_{\pm}/L$ of transmission S-parameters normalized per unit length, expressed in dB·cm^{-1}. A significant isolation between forward

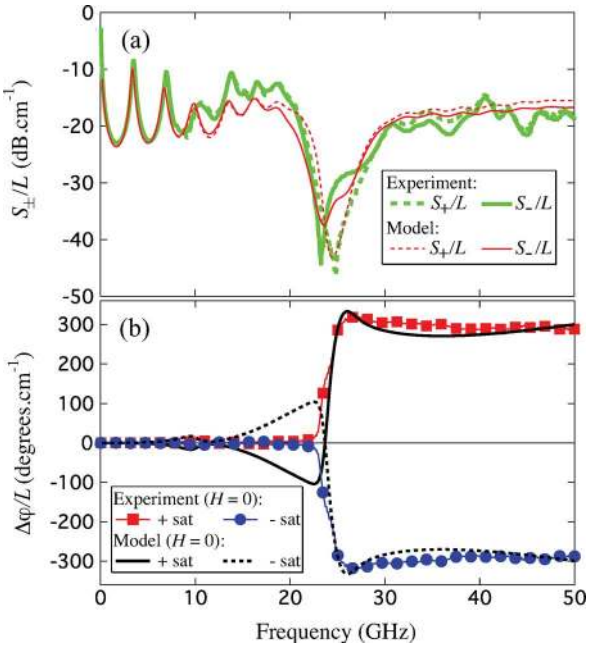

Fig. 3. (a) Measured (thick lines) and calculated (thin lines) S_+/L (dashed lines) and S_-/L (continuous lines) for the NRML of Fig. 1(b) at zero dc biasing magnetic field. (b) Measured (symbols) and calculated (lines) $\Delta\varphi/L$ at zero field for the NRML of (a).

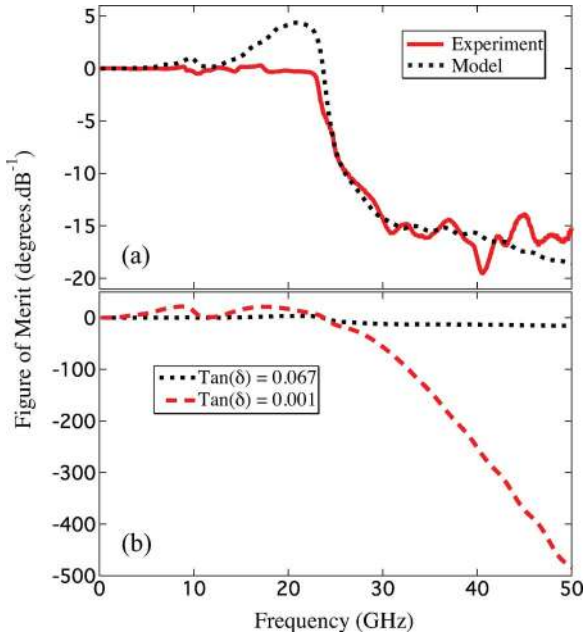

Fig. 4. (a) Measured (continuous line) and calculated (dotted line) FOM at zero field after saturating the NRML of Fig. 1(a) in a positive magnetic field. (b) Calculated FOM for $\tan\delta = 0.067$ (dotted line, same as dotted line of Fig. 4(a) for actual device) and for $\tan\delta = 0.001$ with perfect matching of NRML (dashed line).

and reverse S-parameters is observed around the resonance frequency for CoFe at $f_c = 22.32$ GHz, in both experimental and simulated curves. In simulations, the loss tangent factor is set to $\tan\delta = 0.067$, corresponding to the commercial Synkera substrate, which explains the high insertion losses over the whole frequency range. Such a high value for dielectric losses in alumina is explained by the imperfect purity of the commercial membrane and its amorphous and not crystalline structure resulting from the anodization fabrication procedure, which might also allow the presence of residual bound water molecules in its nanoporous structure [24], [25]. A more significant FMR absorption is present in both propagation directions around the f_c frequency and not at $f_n = 9.95$ GHz, which may be ascribed to the fact that $M_{s_c} > M_{s_n}$ and then the absorption due to NiFe NWs is much lower than that for the CoFe NWs. Furthermore, the isolation of about 18 dB observed around this frequency between forward and reverse transmission clearly indicates a nonreciprocal behavior of the device. It is worth mentioning that resonant transmission peaks observed below 15 GHz are due to unperfect matching offered by tapered edges of the microstrip line at low frequency: because of their small length ($L_T = 2$ mm) with respect to corresponding wavelengths, quarter-wavelength matching to 50-Ω reference impedance is not ensured below 15 GHz.

Interestingly, the measured differential phase shift per unit length $\Delta\varphi/L = (\varphi_+ - \varphi_-)/L$ of the NRML of Fig. 3(b) (squares), where $\varphi_\pm$ is the phase of the $S_\pm$ parameter, is negligible for $f < f_c$ but suddenly increases for $f > f_c$ up to the value 300 degrees·cm^{-1}. Furthermore this value is higher than those reported for devices based on ferrites in the range 38–130 degrees·cm^{-1} at X-band and 300 K [19], [20], [27]–[29]. It is worth mentioning that the high $\Delta\varphi/L$ value obtained without the application of a dc magnetic field in our device is suitable for the realization of a gyrator element ($\Delta\varphi = 180$ degrees) operating in the frequency range 30–50 GHz, which can be obtained with a shorter microstrip line having a length of 0.72 cm. The $\Delta\varphi/L$ calculated from simulated $S_\pm$-parameters (continuous line) predicts negative values close below f_c that are not observed experimentally, however, it agrees well with the measured one above this frequency value. As explained before, either if the sign of the propagation constant k_z is reversed by inverting the propagation direction, or the sign of the off-diagonal term of the permeability tensor $j\kappa_i$ is changed by reversing the magnetization direction, an inversion of the field patterns occurs. Particularly, inverting the sign of $j\kappa_i$ by virtue of a change of sign in m_i [see (4)] leads to an inversion of $\Delta\varphi/L$ as seen by the dashed line in Fig. 3(b). Experimentally, $\Delta\varphi/L$ (circles) is inverted by magnetizing the NRML via the application of a saturating dc field in the opposite direction which is subsequently relaxed to zero. As seen in Fig. 3(b), the most striking feature is that $\Delta\varphi/L$ remains practically constant above f_c where insertion losses are reduced with respect to those at the FMR absorption for CoFe NWs. This means that, in that frequency range, the present device has improved performances as a nonreciprocal phase shifter. As seen in Fig. 4(a), the figure of merit (FOM) $= 2\Delta\varphi/(S_+ + S_-)$ reaches values of about ± 15 degrees·dB^{-1} in the frequency range 30–50 GHz, and both the experimental (continuous line) and calculated (dotted line) values are in good agreement.

V. Parametric Study and Optimization

Simulations in Figs. 3 and 4(a) take into account the ohmic losses of microstrip and ground metallizations as well as the conductivity of the nanowires. We have however demonstrated

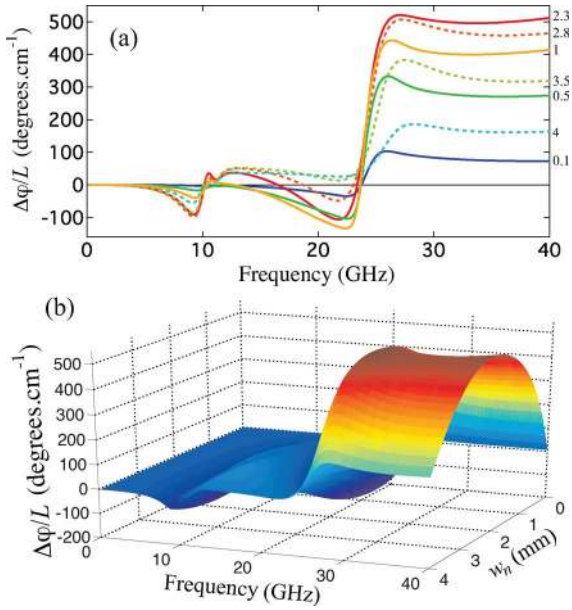

Fig. 5. Calculated $\Delta\varphi/L$ as a function of frequency and width w_n of the NiFe NWs zone such that $w = w_n + w_c = 4.5$ mm, with w_c the width of the CoFe NWs zone. (a) 2-D view. (b) 3-D view. Numbers in (a) correspond to values of w_n in millimeters.

previously in [23] that the loss tangent factor of nanowired substrate does not increase with the presence of conductive metallic nanowires far away from the ferromagnetic resonance. Improving the matching (i.e., optimizing the geometry of tapers to ensure a perfect matching to 50 Ω) will also reduce insertion losses. High dielectric loss reported in the literature for porous alumina is thus the remaining issue to solve, for example, by increasing alumina purity and performing some annealing to avoid residual moisture. FOM performances can be further improved by reducing insertion losses on $S_{\pm}$ that are mainly due to dielectric losses of the PAA membrane, with a residual part induced by mismatch. Indeed, higher FOM of up to 480 degrees·dB^{-1} can be obtained using a high-purity PAA membrane with $\tan\delta = 0.001$, together with a perfect matching of the NRML section to 50 Ω [Fig. 4(b)]. Therefore, improved performances are expected for lower $\tan\delta$ values in the frequency range above the main FMR absorption, which in this case corresponds to the one for the CoFe NWs.

On the other hand, the good agreement between experimental and calculated insertion losses and differential phase shift observed in Fig. 3 suggests that the proposed model allows to predict with good accuracy the microwave properties of our NRML. As an example, our model also shows that these properties can be tuned just by moving the position of the microstrip line in the x-direction perpendicular to the propagation direction or equivalently by changing the widths of the NiFe and CoFe NWs zones beneath the microstrip. The tunable feature of the NRML of Fig. 1 is observed in Fig. 5(a) from the variation of $\Delta\varphi/L$ with the width w_n (numbers at the right vertical axis) of the NiFe NWs zone via the relation $w_n = w - w_c$ with $w = 4.5$ mm. As observed in this figure, $\Delta\varphi/L$ increases in the frequency range $f > f_c$ as w_n increases below 2.3 mm (continuous lines) and decreases above this value (dashed lines). The maximum attainable $\Delta\varphi/L$ value is predicted to be about 500 degrees·cm^{-1} at $w_n = 2.3$ mm, which can be reached just by adjusting during the design the position of the microstrip line along the x-axis of the structure instead of adjusting its length L_w. A 3-D view of the variation of $\Delta\varphi/L$ on f and w_n is shown in Fig. 5(b), where it is seen that introducing a magnetic material beneath the microstrip line with different magnetization than the one already present leads to significant changes in $\Delta\varphi/L$ for $f > f_c$, where insertion losses are lower. Keeping constant the height of both the NiFe and CoFe NWs allows fabricating a tunable phase shifter where $\Delta\varphi$ can be varied using the same device, which can be achieved just by moving the microstrip line as mentioned above.

Finally, the $\Delta\varphi/L$ performances of our device are comparable to those reported for ferrite-superconductor devices [30], [31] for which $\Delta\varphi$ is as high as 1000 degrees in a 2.5-cm-long meaderline leading to $\Delta\varphi/L$ as high as 400 degrees·cm^{-1} at X-band. Even if the FOM of our device is still low, due to the loss tangent factor of the commercial alumina membrane and its not yet optimized matching, our device has the advantage that its frequency of operation lies at Ka-band, suitable for high-frequency microwave applications.

VI. Conclusion

We have proposed a novel planar nonreciprocal microwave device fabricated using a magnetic nanowired substrate and based on a field-displacement mechanism. The nonreciprocal operation of the proposed device results in improved differential phase-shift performances of up to 300 degrees·cm^{-1} at zero applied bias field, which makes it suitable for compact gyrators. This is achieved by controlling the phase velocity of the microwave signal passing through the device via a variation of the MNWS permeability. Finally, the microwave performances simulated using the proposed transmission line model agree with very good accuracy with the experimental results. Further tuning of our device capabilities, like the dependence of the differential phase shift on the relative width of both NW zones, have been predicted.

References

[1] E. Schloemann, "Advances in ferrite microwave materials and devices," *J. Magn. Magn. Mater.*, vol. 209, pp. 15–20, Jan. 2000.
[2] V. G. Harris, A. Geiler, Y. Chen, S. D. Yoon, M. Wu, A. Yang, Z. Chen, P. He, P. V. Parimi, X. Zuo, C. E. Patton, M. Abe, O. Acher, and C. Vittoria, "Recent advances in processing and applications of microwave ferrites," *J. Magn. Magn. Mater.*, vol. 321, pp. 2035–2047, Jan. 2009.
[3] J. D. Adam, L. E. Davis, G. F. Dionne, E. F. Schloemann, and S. N. Stitzer, "Ferrite devices and materials," *IEEE Trans. Microw. Theory Tech.*, vol. 50, no. 3, pp. 721–737, Mar. 2002.
[4] S. A. Oliver, P. Shi, W. Hu, H. How, S. W. McKnight, N. E. McGruer, P. M. Zavracky, and C. Vittoria, "Integrated self-biased hexaferrite microstrip circulators for millimeter-wavelength applications," *IEEE Trans. Microw. Theory Tech.*, vol. 49, no. 2, pp. 385–387, Feb. 2001.
[5] G. Goglio, S. Pignard, A. Radulescu, L. Piraux, I. Huynen, D. Vanhoenacker, and A. Vander Vorst, "Microwave properties of metallic nanowires," *Appl. Phys. Lett.*, vol. 75, pp. 1769–1771, Jul. 1999.
[6] A. Encinas-Oropesa, M. Demand, L. Piraux, I. Huynen, and U. Ebels, "Dipolar interactions in arrays of nickel nanowires studied by ferromagnetic resonance," *Phys. Rev. B*, vol. 63, Feb. 2001, Art. ID 104415.
[7] J. De La Torre Medina, L. Piraux, J. M. O. Govea, and A. Encinas, "Double ferromagnetic resonance and configuration-dependent dipolar coupling in unsaturated arrays of bistable magnetic nanowires," *Phys. Rev. B*, vol. 81, Apr. 2010, Art. ID 144411.

[8] A. Sklyuyev, M. Ciureanu, C. Akyel, P. Ciureanu, and A. Yelon, "Microwave studies of magnetic anisotropy of Co nanowire arrays," *J. Appl. Phys.*, vol. 105, Jan. 2009, Art. ID 023914.
[9] R. L. Marson, B. K. Kuanr, S. R. Mishra, R. E. Camley, and Z. Celinski, "Nickel nanowires for planer microwave circuit applications and characterization," *J. Vac. Sci. Tech. B*, vol. 25, pp. 2619–2623, Nov. 2007.
[10] A. Saib, M. Darques, L. Piraux, D. Vanhoenacker-Janvier, and I. Huynen, "Unbiased microwave circulator based on ferromagnetic nanowires arrays of tunable magnetization state," *J. Phys. D: Appl. Phys.*, vol. 38, pp. 2759–2763, Aug. 2005.
[11] A. Saib, M. Darques, L. Piraux, D. Vanhoenacker-Janvier, and I. Huynen, "An unbiased integrated microstrip circulator based on magnetic nanowired substrate," *IEEE Trans. Microw. Theory Tech.*, vol. 53, no. 6, pp. 2043–2049, Jun. 2005.
[12] M. Darques, J. De la Torre Medina, L. Piraux, L. Cagnon, and I. Huynen, "Microwave circulator based on ferromagnetic nanowires in an alumina template," *Nanotech.*, vol. 12, Mar. 2010, Art. ID 145208.
[13] J.-F. Allaeys and J.-C. Mage, "Numerical modelling of unbiased microstrip circulators based on magnetic nanowired substrate: Use of a ferrite-equivalent model," in *IEEE MTT-S Int. Microw. Symp. Dig.*, Jul. 2007, pp. 703–706.
[14] B. K. Kuanr, V. Veerakumar, R. Marson, S. R. Mishra, R. E. Camley, and Z. J. Celinski, "Nonreciprocal microwave devices based on magnetic nanowires," *Appl. Phys. Lett.*, vol. 94, May 2009, Art. ID 202505.
[15] L.-P. Carignan, C. Caloz, and D. Menard, "Dual-band integrated self-biased edge-mode isolator based on the double ferromagnetic resonance of a bistable nanowire substrate," in *IEEE MTT-S Int. Microw. Symp. Dig.*, Jul. 2010, pp. 1336–1339.
[16] J. De La Torre Medina, J. Spiegel, M. Darques, L. Piraux, and I. Huynen, "Differential phase shift in nonreciprocal microstrip lines on magnetic nanowired substrates," *Appl. Phys. Lett.*, vol. 96, Feb. 2010, Art. ID 072508.
[17] C. E. C. González, J. De La Torre Medina, A. Encinas, and L. Piraux, "Electrodeposition growth of nanowire arrays with height gradient profiles for microwave device applications," *Nano Lett.*, vol. 11, pp. 2023–2027, Apr. 2011.
[18] M. E. Hines, "Reciprocal and nonreciprocal modes of propagation in ferrite stripline and microstrip devices," *IEEE Trans. Microw. Theory Tech.*, vol. MMT-19, no. 5, pp. 442–451, May 1971.
[19] J. Zafar, A. A. P. Gibson, and H. R. Zafar, "High power ferrite phase shifter for beam steering applications," in *Proc. 3rd Eur. Conf. Antennas Propagation*, 2009, p. 3029.
[20] J. Mielewski and A. Buda, "Analysis of the nonreciprocal ferrite phase shifter with nonuniform cross-section," in *Proc. 12th Int. Conf. Microw. Radar*, 1998, vol. 2, pp. 509–513.
[21] B. Lax and K. J. Button, *Microwave Ferrites and Ferrimagnetics*, 1st ed. New York: McGraw-Hill, 1962.
[22] R. Marqués, F. Mesa, and F. Medina, "Theory of magnetoelectric multiconductor transmission lines with application to chiral and gyrotropic lines," *Microw. Opt. Technol. Lett.*, vol. 38, pp. 3–9, Jul. 2003.
[23] J. Spiegel, J. De La Torre Medina, M. Darques, L. Piraux, and I. Huynen, "Permittivity model for ferromagnetic nanowired substrates," *IEEE Microw. Wireless Comp. Lett.*, vol. 17, no. 7, pp. 492–494, Jul. 2007.
[24] S. J. Perm, N. McN. ALford, A. Templeton, X. Wang, M. Xu, M. Reece, and K. Schrape, "Effect of porosity and grain size on the microwave dielectric properties of sintered alumina," *J. Amer. Ceram. Soc.*, vol. 80, pp. 1185–1188, 1997.
[25] J. Mollá, M. González, R. Vila, and A. Ibara, "Effect of humidity on microwave dielectric losses of porous alumina," *J. Appl. Phys.*, vol. 85, pp. 1727–1730, Feb. 1999.
[26] P. Quéffélec, S. Mallégol, and M. Le Floc'h, "Automatic measurement of complex tensorial permeability of magnetized materials in a wide microwave frequency range," *IEEE Trans. Microw. Theory Tech.*, vol. MTT-50, no. 9, pp. 2128–2134, Sep. 2002.
[27] C. P. Wen, "Coplanar waveguide: A surface strip transmission line suitable for nonreciprocal gyromagnetic device applications," *IEEE Trans. Microw. Theory Tech.*, vol. MTT–17, no. 12, pp. 1087–1090, Dec. 1969.
[28] W. Junding, Y.-Z. Xiong, M.-J. Shi, G.-F. Chen, and M.-D. Yu, "Analysis of twin ferrite toroidal phase shifter in grooved waveguide," *IEEE Trans. Microw. Theory Tech.*, vol. 42, no. 4, pp. 616–621, Apr. 1994.
[29] W. Che, E. K.-N. Yung, S. Chen, and J. Wen, "Improved analysis of nonreciprocal remanence ferrite phase shifter in grooved waveguide," *IEEE Trans. Microw. Theory Tech.*, vol. 50, no. 8, pp. 1912–1918, Aug. 2002.
[30] G. F. Dionne, D. E. Oates, D. H. Temme, and J. A. Weiss, "Ferrite-superconductor devices for advanced microwave applications," *IEEE Trans. Microw. Theory Tech.*, vol. 44, no. 7, pp. 1361–1368, Jul. 1996.
[31] G. F. Dionne, D. E. Oates, D. H. Temme, and J. A. Weiss, "Superconductor ferrite phase shifters and circulators," *IEEE Trans. Appl. Superconduct.*, vol. 7, no. 6, pp. 2347–2350, Jun. 1995.

Gaël Hamoir was born in Liège, Belgium, in 1985. He received the Civil Engineering degree from the École Polytechnique de Louvain, Louvain-la-Neuve, Belgium, in 2009. He is currently working toward the Ph.D. degree in engineering at the Université Catholique de Louvain, Louvain-la-Neuve.

Since 2009, he has been with the Bio- and Soft-Matter Group, Institute of Condensed Matter and Nanosciences, Université Catholique de Louvain, Louvain-la-Neuve, Belgium. His main research concerns the modeling, conception, and characterization of devices based on ferromagnetic nanowire arrays.

Joaquin De La Torre Medina was born in Aguascalientes, Mexico, in 1979. He received the degree in applied mathematics from the Universidad Autónoma de San Luis Potosi, San Luis Potosi, Mexico, and the Ph.D. degree in applied sciences from the Université Catholique de Louvain, Louvain-la-Neuve, Belgium, in 2009.

He was with the Université Catholique de Louvain, Louvain-la-Neuve, Belgium, and with the Universidad Autonoma de San Luis Potosi, San Luis Potosi, Mexico, in postdoctoral positions in 2010 and 2011, respectively. In 2012, he joined the Physics and Mathematics Faculty, Universidad Michoacana de San Nicolás de Hidalgo, Morelia, Mexico, as a Full Professor. His research concerns magnetism of nanocomposite materials and microwave devices based on arrays of magnetic nanowires.

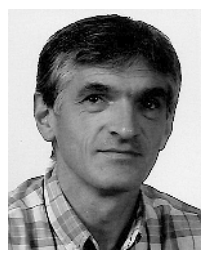

Luc Piraux received the Ph.D. degree from the University of Louvain, Louvan-la-Neuve, Belgium, in 1987.

He was a Research Associate with the National Fund for Scientific Research, Belgium, during 1989–2001. Currently with the Institute of Condensed Matter and Nanosciences (ICMN), Université Catholique de Louvain, Louvain-la-Neuve, Belgium, his research activity deals with basic experimental research in the field of nanostructured materials and low-dimensional systems. His research team has expertise in the fabrication of magnetic and superconducting nanowires as well as in the fabrication of highly ordered nanoporous alumina templates. His current research activities are in the field of spintronics, nanomagnetism, low-dimensional superconductivity, vortex dynamics, and development of microwave devices. He has authored and coauthored more than 200 publications in peer-reviewed journals and holds three patents.

Isabella Huynen (S'90–A'95–M'96–SM'06) received the Electrical Engineer degree and Ph.D. degree in applied sciences from the Université Catholique de Louvain, Louvain-la-Neuve, Belgium, in 1989 and 1994, respectively.

In 1989, she joined the Microwave Laboratory, Université Catholique de Louvain, Louvain-la-Neuve, Belgium, where she is currently a part-time Professor. She is also a Research Director with the Research Science Foundation, Brussels, Belgium. She has authored or coauthored one book and over 250 papers in journals and conference proceedings. She holds three patents. Her particular research interests in the development of devices based on nanoscaled materials and topologies for applications at microwave, millimeter-wave, and optical wavelengths.